Distributed Optimal Voltage Control for Multi-terminal Direct Current System with Large-scale Wind Farm Cluster Based on ADMM

Xueping Li, Yinpeng Qu, Jianxin Deng, Sheng Huang, Derong Luo, and Qiuwei Wu

Abstract—**The power loss minimization and DC voltage stability of the multi-terminal direct current (MTDC) system with large-scale wind farm (WF) cluster affect the stability and power quality of the interconnected power grid. This paper proposes a distributed optimal voltage control (DOVC) strategy, which aims to optimize voltage distribution in MTDC and WF systems, reduce system power losses, and track power dispatch commands. The proposed DOVC strategy employs a bi-level distributed control architecture. At the upper level, the MTDC controller coordinates power flow, DC-side voltage of grid-side voltage source converters (GSVSCs), and WF-side voltage source converters (WFVSCs) for power loss minimization and DC voltage stabilization of the MTDC system. At the lower level, the WF controller coordinates the controlled bus voltage of WFVSC and the active and reactive power of wind turbines (WTs) to maintain WT terminal voltages within feasible range. Then, the WF controller minimizes the power loss of the WF system, while tracking the optimal command from the upper-level control strategy. Considering the computational tasks of multi-objective optimization with large-scale WF cluster, the proposed DOVC strategy is executed in a distributed manner based on the alternating direction method of multipliers (ADMM). An MTDC system with large-scale WF cluster is established in MATLAB to validate the effectiveness of the proposed DOVC strategy.**

Index Terms—**Multi-terminal direct current (MTDC), distributed optimal voltage control, voltage source converter, alternating direction method of multipliers (ADMM), wind farm.**

I. Introduction

THE offshore wind power has attracted extensive attention due to its excellent wind energy capture capability and abundant offshore wind energy resources [1]-[3]. With the expansion of offshore wind farms (OWFs), the voltage source converter based high-voltage direct current (VSC-HVDC) system has become an attractive collection and transmission system for large OWFs [4]. As the extended topology of VSC-HVDC, the voltage source converter based multi-terminal direct current (VSC-MTDC) transmission system offers distinct advantages for connecting remote OWFs, including higher transmission capacity, fully controllable power flow, and the ability to facilitate multi-point power supply and reception, surpassing the capabilities of conventional VSC-HVDC [5], [6]. By sharing DC buses, VSC-MTDC enables meshed interconnections between regional power systems and large-scale wind farms (WFs), thereby enhancing system reliability and control flexibility [7], [8]. As a result, the multi-terminal direct current (MTDC) system is well-suited for integrating large-scale WF cluster into the power grid.

As large-scale WF cluster is integrated into the power grid via the MTDC system, the inherent randomness and volatility of wind power, coupled with the lower short-circuit power contribution of wind turbines (WTs) and MTDC converters, can lead to significant voltage fluctuations and even voltage violations under disturbances. Given that the voltage distribution of the power system is influenced by both the power output of WTs within each WF and the power flow among VSCs in the MTDC system, the key to maintaining all bus voltages and WT terminal voltages within a feasible range lies in developing efficient voltage and power regulation control methods.

Voltage and power controls of WFs have been extensively studied in recent years. Reference [9] introduces a model predictive control (MPC)-based method for VSC-HVDC systems, which is aimed at integrating OWFs into power grids while ensuring active/reactive power sharing and efficient regulation of AC voltage across varying operational conditions of different OWFs. An MPC-based voltage control method is proposed in [10] and [11] for OWFs, optimizing the power references of WT and minimizing bus voltage deviations of WF while also accounting for the economic operation of the WF. Reference [12] introduces a novel strategy for optimizing secondary voltage control in high-voltage direct current (HVDC)-connected OWFs, aiming to achieve coordinated control between HVDC systems and WFs to minimize voltage fluctuations. A centralized optimal reactive

Manuscript received: March 19, 2024; revised: July 5, 2024; accepted: October 8, 2024. Date of CrossCheck: October 8, 2024. Date of online publication: November 7, 2024.

This work was supported by the National Key R&D Program of China (No. 2022YFF0608700).

X. Li, Y. Qu (corresponding author), S. Huang, and D. Luo are with the College of Electrical and Information Engineering, Hunan University, Changsha, China (e-mail: lxp1993@hnu.edu.cn; quyinpeng@hnu.edu.cn; huang98123@163.com; hdldr@hnu.edu.cn).

J. Deng is with Guangdong Power Grid Co., Ltd., Dongguan, China (e-mail: jxdeng@hun.edu.cn).

Q. Wu is with the School of Electronics, Electrical Engineering, and Computer Science, Queen's University Belfast, BT8 5BN, Belfast, UK (e-mail: qiuwei.wu@qub.ac.uk).

DOI: 10.35833/MPCE.2024.000298

power dispatch strategy is proposed in [13] to minimize the total losses of the WF, including losses in cables, WT transformers, and wind energy generation systems. Reference [14] presents an MPC-based hierarchical cluster coordination control (HCCC) strategy to handle the complex optimal dispatch and real-time control for large-scale WF cluster. A two-tier optimal voltage control strategy for the large-scale WF cluster is proposed in [15], where the consensus protocol is used in the upper-tier controller, and the lower-tier control is realized using the alternating direction method of multipliers (ADMM) algorithm. In [16], an adaptive droop-based hierarchical optimal voltage control (DHOVC) scheme is proposed for OWFs, which optimizes the droop coefficients of each WT through a decentralized voltage prediction model.

To ensure the stable operation of VSC-MTDC systems, maintaining DC voltage stability is crucial. Generally, control methods for DC voltage regulation in MTDC systems can be classified into two main categories: master-slave methods and voltage droop control methods [17]. In [18], a distributed strategy is proposed for hierarchical control of voltage source converter (VSC) based DC microgrids to achieve proportional power sharing and voltage regulation. An adaptive DC voltage droop control is explored in [19], with the primary goal of minimizing the power-sharing burden on converters during power variations or disturbances, while adhering to the constraints of the DC grid. In [20], an adaptive reference power-based voltage droop control method is introduced, which adjusts the reference power to compensate for power deviations in droop-controlled VSCs. This method decouples the active and reactive power flows between the WF and AC grid, ensuring full controllability and reducing MTDC power losses by regulating the voltage among VSCs. A generic DC grid controller that employs nonlinear constrained optimization techniques is proposed in [21] to optimize the performance of multi-terminal HVDC systems based on various operational objectives, including minimizing grid power loss and operation costs. In [22], a hierarchical control framework is proposed for MTDC system connected to large-scale renewable energy generation. The primary control layer ensures the voltage stability of VSCs linked to the main AC grid, while the secondary control layer focuses on minimizing DC grid power losses and ensuring accurate power sharing among droop-based VSCs. In [23], an optimal control method for power converters is presented, minimizing power losses in the MTDC system and enabling decentralized operation even in the presence of intermittent wind power generation. In [24], setpoints are adjusted based on enhanced AC-DC power flow algorithm, with the dual objectives of minimizing both DC voltage deviation and transmission losses.

However, as the size and number of MTDC and WFs increase, solving a global optimization problem that involves large-scale constraints from both the MTDC system and WFs in real-time becomes increasingly complex and challenging [25]. To address the significant computational burden on the system controller and the need for rapid online response, a distributed voltage control scheme for the MTDC system with large-scale WF cluster is essential [26]. The ADMM algorithm has been widely employed in WFs to manage active and reactive power in a distributed manner, which relies on a limited number of controllers to exchange information, demonstrating strong computational efficiency [13], [15], [27], [28]. In [27], a decentralized coordinated voltage control scheme (DCVCS) for VSC-HVDC-connected WFs is proposed, utilizing a decentralized solution based on ADMM to solve the MPC problem. Similarly, [28] introduces an ADMM-based hierarchical optimal active power control (HOAPC) scheme for the synthetic inertial response of large-scale WF cluster, solving the MPC-based optimization problem in a fast way.

Most of existing voltage optimization control strategies are designed for AC WFs or VSC-HVDC-connected WFs, with a limited focus on voltage regulation for MTDC systems with large-scale WF cluster. The optimization of the VSC-MTDC system and the power tracking for GSVSC are often neglected, which can significantly impact both the economic operation and stability of the power system. The coordination between WFs and the MTDC system is essential to achieve optimal operation across the entire system. As WFs and MTDC systems expand, developing fast and efficient solutions to large-scale optimization problems becomes crucial for achieving real-time system optimization. This paper proposes a distributed optimal voltage control (DOVC) strategy for the MTDC system with large-scale WF cluster based on ADMM. The model of the MTDC system with large-scale WF cluster includes the WT, the WF-side voltage source converters (WFVSC), and the grid-side voltage source converter (GSVSC) models. The DOVC strategy aims to maintain the voltages of WTs inside each WF and VSCs of the MTDC system within a feasible range while minimizing the overall grid power losses. The global optimization problem is divided into subproblems, which are solved in parallel using the ADMM on MTDC and WF controllers, respectively. Through the proposed DOVC strategy, the MTDC controller and WF controllers solve the optimization problem in a distributed manner, ensuring global optimality without any compromise. The main contributions of this paper are summarized as follows:

1) A DOVC strategy for the MTDC system with large-scale WF cluster is proposed to achieve voltage regulation for the VSCs of MTDC and WTs within WFs while minimizing grid power losses in both the MTDC system and WF cluster. The entire system, including the WT, the WFVSC, and the GSVSC models, is established. Through the proposed DOVC strategy, WT power output and the DC-side voltage of the VSCs are coordinated to realize effective control performance for the entire system.

2) A bi-level distributed control architecture is designed. The upper-level MTDC controller solves the optimization problem related solely to the MTDC system and updates the global variables with global constraints, while each lower-level WF controller addresses the optimal problem under local variable constraints. This method reduces control complexity and ensures global optimization across the entire system.

3) To efficiently solve the large-scale multi-objective opti-

mization problem for the MTDC system connected to the WF cluster, an ADMM-based solution method is proposed to execute the proposed DOVC strategy to distribute the computational burden of multi-objective optimizations. Each WF controller only exchanges information with the MTDC controller, and certain information between the WF controller and WT controllers is exchanged, enhancing system privacy and reducing data exchange requirements.

The rest of this paper is organized as follows. Section II provides a DOVC strategy architecture. Section III introduces the mathematical model of the MTDC system with large-scale WF cluster. Then, the framework of the DOVC strategy and the ADMM-based solution are given in Section IV. Simulation results are presented and discussed in Section V. Finally, the conclusions are drawn in Section VI.

II. DOVC Strategy Architecture

A. Configuration of MTDC System with Large-scale WF Cluster

Figure 1 shows the configuration of an MTDC system with large-scale WF cluster with N_{W} WTs, which connects to a 400 kV onshore AC grid through a 400 kV MTDC system.

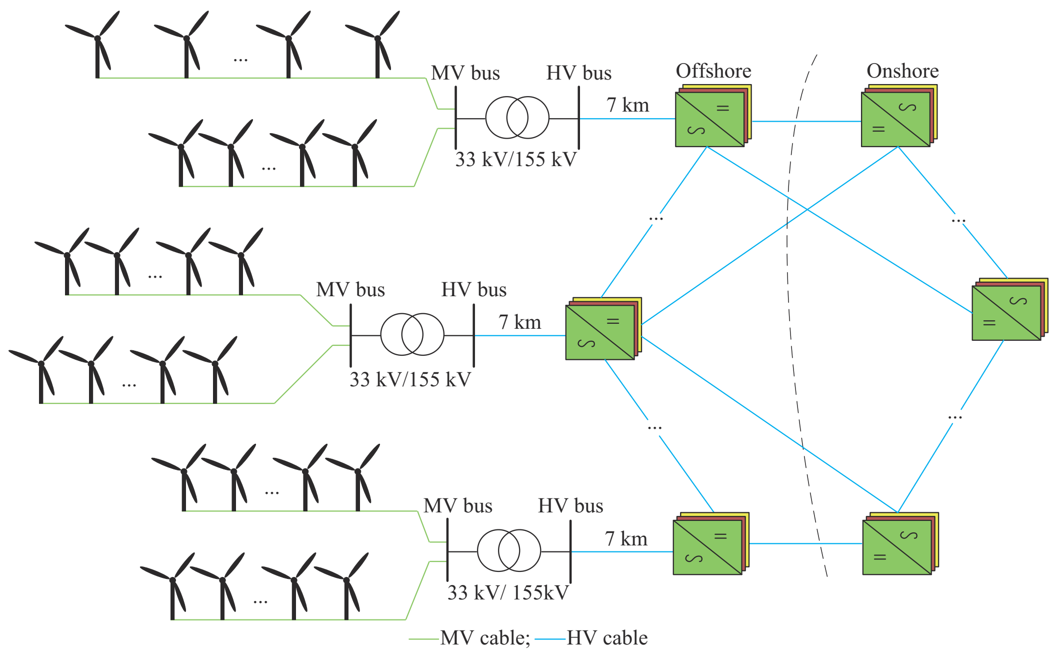

Fig. 1. Configuration of an MTDC system with large-scale WF cluster.

The MTDC system forms a meshed grid comprising $|\mathcal{M}|$ WFVSCs and $|\mathcal{W}|$ GSVSCs. Each WF is connected to a WFVSC via an high-voltage (HV) or medium-voltage (MV) transformer. The WFVSC is responsible for providing stable slack bus voltage for the WF and transferring the wind power from the WF side to the MTDC system. The GSVSC converts the DC power output from WFVSC into three-phase AC power for direct connection to the AC grid, which is responsible for transmitting offshore power from the MTDC system to the onshore AC grid. The interconnected VSCs of the MTDC system are connected through HV cables, while each WFVSC is connected to its corresponding WF through 155 kV submarine cables. The WTs are interconnected via MV 33 kV collector cables, with the WTs spaced 4 km apart.

B. Proposed DOVC Strategy

The DOVC control structure is illustrated in Fig. 2, which is divided into two parts: MTDC control and WF control. In Fig. 2, $i \in \mathcal{M}$, $\boldsymbol{P}_{\mathrm{W}}^{i}$ and $\boldsymbol{Q}_{\mathrm{W}}^{i}$ are the active and reactive power vectors of WTs in the i^{th} WF, respectively; $\boldsymbol{P}_{\mathrm{W}}^{\mathrm{ref},i}$ and $\boldsymbol{Q}_{\mathrm{W}}^{\mathrm{ref},i}$ are the active and reactive power reference vectors of WTs in the i^{th} WF, respectively; $\boldsymbol{V}_{\mathrm{W}}^{i}$ and $\boldsymbol{\theta}_{\mathrm{W}}^{i}$ are the amplitude vector and phase angle vector of the WT terminal voltage in the i^{th} WF, respectively; $P_{\mathrm{TSO},i}^{\mathrm{ref}}$ is the scheduling active power output command of the i^{th} GSVSC; $\boldsymbol{u}_{\mathrm{WV,dc}}^{i}$ is the DC-side voltage vector of the i^{th} WFVSC; $\boldsymbol{u}_{\mathrm{GV,dc}}^{\mathrm{ref},i}$ is the optimal voltage reference vector of the i^{th} GSVSCs; $u_{\mathrm{S}}^{\mathrm{ref},i}$ is the bus voltage reference on the WF side; $Z_{g,i}$ is the power reference of the i^{th} WF; $Z_{\mathrm{l},i}$ and γ_i are the local and dual variables received from the WF controllers, respectively; and $\boldsymbol{u}_{\mathrm{GV,dc}}^{i}$ is the DC side voltage vector of the i^{th} GSVSC. The upper-level controller coordinates the VSCs within the MTDC system to minimize grid power losses across the MTDC system. It generates optimal voltage reference vectors for both $\boldsymbol{u}_{\mathrm{GV,dc}}^{\mathrm{ref},i}$ and $\boldsymbol{u}_{\mathrm{WV,dc}}^{\mathrm{ref},i}$, ensuring that each GSVSC can track dispatch commands from the transmission system operator (TSO) based on the optimal power flow within MTDC system.

According to the power balance theorem, the upper-level controller calculates the active power reference for each WF and sends it to the lower-level WF controller. The lower-level WF controller regulates $u_{\mathrm{S}}^{\mathrm{ref},i}$ and manages the active and reactive power references for WTs within each WF, aiming to keep $u_{\mathrm{S}}^{\mathrm{ref},i}$ within feasible ranges, minimize power losses for WF system, and track the active power commands from the upper-level controller.

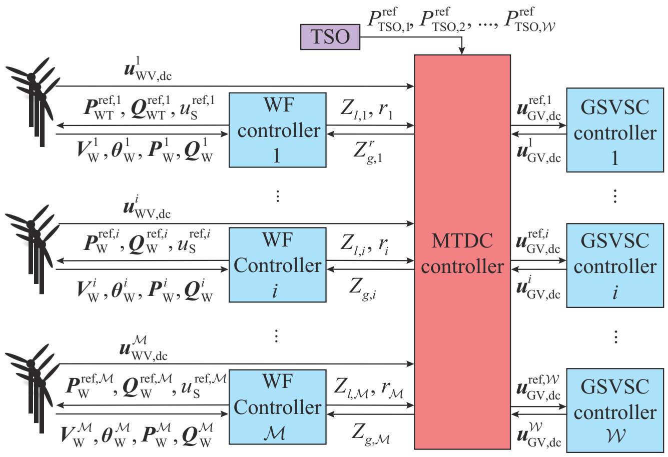

Fig. 2. DOVC control structure.

To reduce the computational burden on the system, the global optimal control problem is divided into subproblems, which are solved in parallel by the MTDC and WF controllers using the ADMM framework. Each WF controller only exchanges limited information with the MTDC controller. The MTDC controller continuously solves for $Z_{g,i}$, and distributes them to the WF controllers based on $Z_{l,i}$ and γ_i received from the WF controllers.

III. Proposed Control Strategy

In this section, the model of the MTDC system with large-scale WF cluster is introduced. The simplified structure of the MTDC system with large-scale WF cluster is shown in Fig. 3, comprising WFVSCs, GSVSCs, the DC grid, and WFs. The mathematical models for the WT, WFVSC, and GSVSC are established in this section.

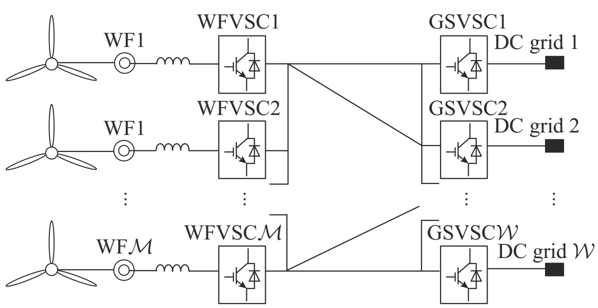

Fig. 3. Simplified structure of MTDC system with large-scale WF cluster.

A. Model of WFVSC

The voltage and current dual closed-loop control structure of the WFVSC is illustrated in Fig. 4, where PWM is short for pulse width modulation. The outer loop of the WFVSC controller utilizes fixed AC voltage amplitude control to ensure stable AC voltage for the WF system.

The three-phase AC voltage is decoupled into *d*-*q* axis components for independent control, and the simplified voltage control structure of the WFVSC is presented, as shown in Fig. 5. The time delay is modeled using a 1st-order lag function with a time constant of T^{d}. All the variables in the Figs. 4 and 5 can be found in [10].

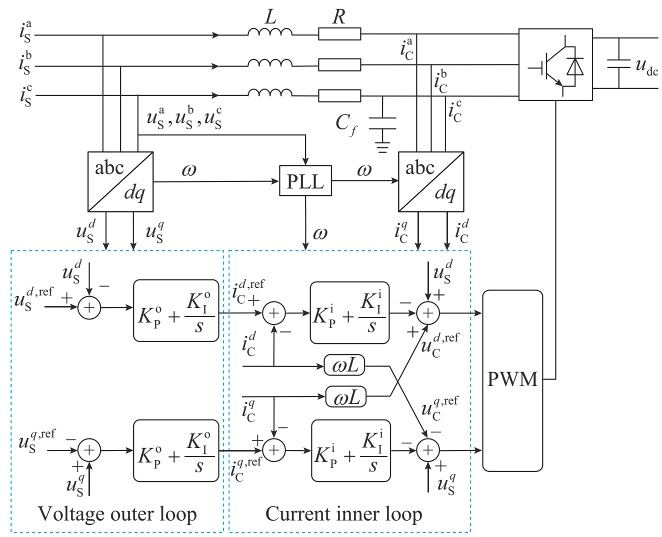

Fig. 4. Voltage and current dual closed-loop control structure of WFVSC.

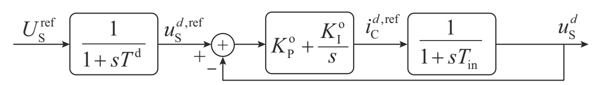

Fig. 5. Simplified voltage control structure of WFVSC.

The mathematical model of WFVSC can be described by:

$$\Delta u_{\mathrm{S}}^{d,\mathrm{ref}} = \frac{1}{1+sT^{\mathrm{d}}}\Delta U_{\mathrm{S}}^{\mathrm{ref}} \tag{1}$$

$$\Delta u_{\mathrm{S}}^{d,\mathrm{I}} = \frac{K_{\mathrm{I}}^{\mathrm{o}}}{s}(\Delta u_{\mathrm{S}}^{d,\mathrm{ref}} - \Delta u_{\mathrm{S}}^{d}) \tag{2}$$

$$\Delta u_{\mathrm{S}}^{d} = \frac{1}{1+sT_{\mathrm{in}}}\left(K_{\mathrm{P}}^{\mathrm{o}} + \frac{K_{\mathrm{I}}^{\mathrm{o}}}{s}\right)(\Delta u_{\mathrm{S}}^{d,\mathrm{ref}} - \Delta u_{\mathrm{S}}^{d}) \tag{3}$$

where $\Delta U_{\mathrm{S}}^{\mathrm{ref}} = U_{\mathrm{S}}^{\mathrm{ref}} - U_{\mathrm{S}}^{\mathrm{ref}}(t_0)$ is the controlled bus voltage reference increment, with superscript ref indicating the reference value and t_0 indicating the initial time; $\Delta u_{\mathrm{S}}^{d} = u_{\mathrm{S}}^{d} - u_{\mathrm{S}}^{d}(t_0)$ is the increment of the *d*-axis component of the controlled bus voltage of WFVSC; $\Delta u_{\mathrm{S}}^{d,\mathrm{I}} = u_{\mathrm{S}}^{d,\mathrm{ref}} - u_{\mathrm{S}}^{d}$ is the auxiliary variable, denoting the integral gain of $u_{\mathrm{S}}^{d,\mathrm{ref}} - u_{\mathrm{S}}^{d}$; $K_{\mathrm{P}}^{\mathrm{o}}$ and $K_{\mathrm{I}}^{\mathrm{o}}$ are the proportional and integral gains of the proportional integral (PI) controllers of the outer control loop, respectively; and T_{in} is the time constant for the inner loop.

According to (1)-(3), the mathematical model of the continuous state space model of WFVSC can be formulated as:

$$\dot{\boldsymbol{x}}_{\mathrm{WV}} = \boldsymbol{A}_{\mathrm{WV}}\boldsymbol{x}_{\mathrm{WV}} + \boldsymbol{B}_{\mathrm{WV}}\boldsymbol{u}_{\mathrm{WV}} \tag{4a}$$

$$\boldsymbol{A}_{\mathrm{WV}} = \begin{bmatrix} -\dfrac{1}{T^{\mathrm{d}}} & 0 & 0 \\ K_{\mathrm{I}}^{\mathrm{o}} & 0 & -K_{\mathrm{I}}^{\mathrm{o}} \\ \dfrac{K_{\mathrm{P}}^{\mathrm{o}}}{T_{\mathrm{in}}} & \dfrac{1}{T_{\mathrm{in}}} & -\dfrac{1+K_{\mathrm{P}}^{\mathrm{o}}}{T_{\mathrm{in}}} \end{bmatrix} \tag{4b}$$

$$\boldsymbol{B}_{\mathrm{WV}} = \begin{bmatrix} \dfrac{1}{T^{\mathrm{d}}} \\ 0 \\ 0 \end{bmatrix} \tag{4c}$$

where $\boldsymbol{x}_{\mathrm{WV}} = [\Delta u_{\mathrm{S}}^{d,\mathrm{ref}}, \Delta u_{\mathrm{S}}^{d,\mathrm{I}}, \Delta u_{\mathrm{S}}^{d}]^{\mathrm{T}}$ is the state variable vector of the WFVSC system; $\boldsymbol{u}_{\mathrm{WV}}=[\Delta U_{\mathrm{S}}^{\mathrm{ref}}]$ is the control variable; $\boldsymbol{A}_{\mathrm{WV}}$ is the state matrix; and $\boldsymbol{B}_{\mathrm{WV}}$ is the control matrix.

B. Model of GSVSC

The voltage control structure of the GSVSC is shown in Fig. 6. GSVSC utilizes a fixed DC voltage control method to stabilize the bus voltage in the DC system and facilitate coordinated control of the MTDC system. The simplified voltage control structure of the GSVSC is shown in Fig. 7.

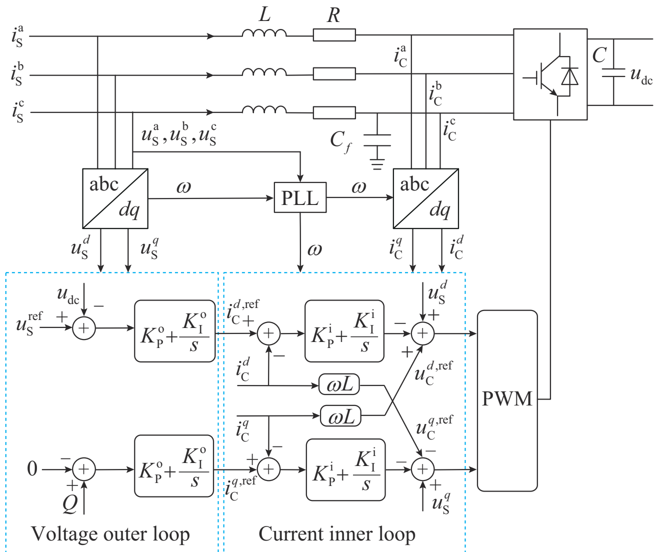

Fig. 6. Voltage control structure of GSVSC.

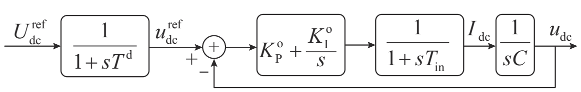

Fig. 7. Simplified voltage control structure of GSVSC.

Unlike the WFVSC, the DC-side voltage of GSVSC is measured after being filtered by a capacitor. As a result, a capacitor filtering stage is incorporated before obtaining the DC-side voltage measurement for the GSVSC. The mathematical model of the GSVSC can be expressed as:

$$u_{\mathrm{dc}}^{\mathrm{ref}}=\frac{1}{1+sT^{\mathrm{d}}}U_{\mathrm{dc}}^{\mathrm{ref}} \tag{5}$$

$$u_{\mathrm{dc}}^{\mathrm{I}}=\frac{K_{\mathrm{I}}^{\mathrm{o}}}{s}(u_{\mathrm{dc}}^{\mathrm{ref}}-u_{\mathrm{dc}}) \tag{6}$$

$$I_{\mathrm{dc}}=\frac{K_{\mathrm{P}}^{\mathrm{o}}}{1+sT_{\mathrm{in}}}(u_{\mathrm{dc}}^{\mathrm{ref}}-u_{\mathrm{dc}})+\frac{1}{1+sT_{\mathrm{in}}}u_{\mathrm{dc}}^{\mathrm{I}} \tag{7}$$

$$u_{\mathrm{dc}}=\frac{1}{sC}I_{\mathrm{dc}} \tag{8}$$

where I_{dc} and u_{dc} are the current and voltage on the DC side of GSVSC, respectively; $U_{\mathrm{dc}}^{\mathrm{ref}}$ is the DC-side voltage reference of GSVSC sent by the MTDC; $u_{\mathrm{dc}}^{\mathrm{I}}$ is the introduced auxiliary variable denoting the integral gain of $u_{\mathrm{dc}}^{\mathrm{ref}}-u_{\mathrm{dc}}$; and C is the capacitance of the DC-side capacitor.

According to (5)-(8), the mathematical model of the continuous state space model of GSVSC can be obtained as:

$$\dot{\boldsymbol{x}}_{\mathrm{GV}}=\boldsymbol{A}_{\mathrm{GV}}\boldsymbol{x}_{\mathrm{GV}}+\boldsymbol{B}_{\mathrm{GV}}\boldsymbol{u}_{\mathrm{GV}} \tag{9a}$$

$$\boldsymbol{A}_{\mathrm{GV}}=\begin{bmatrix} -\frac{1}{T^{\mathrm{d}}} & 0 & 0 & 0 \\ K_{\mathrm{I}}^{\mathrm{o}} & 0 & 0 & -K_{\mathrm{I}}^{\mathrm{o}} \\ \frac{K_{\mathrm{P}}^{\mathrm{o}}}{T_{\mathrm{in}}} & \frac{1}{T_{\mathrm{in}}} & -\frac{1}{T_{\mathrm{in}}} & -\frac{K_{\mathrm{P}}^{\mathrm{o}}}{T_{\mathrm{in}}} \\ 0 & 0 & \frac{1}{sC} & 0 \end{bmatrix} \tag{9b}$$

$$\boldsymbol{B}_{\mathrm{GV}}=\begin{bmatrix} \frac{1}{T^{\mathrm{d}}} \\ 0 \\ 0 \\ 0 \end{bmatrix} \tag{9c}$$

where $\boldsymbol{x}_{\mathrm{GV}}=[u_{\mathrm{dc}}^{\mathrm{ref}}, u_{\mathrm{dc}}^{\mathrm{I}}, I_{\mathrm{dc}}, u_{\mathrm{dc}}]^{\mathrm{T}}$ is the state variable vector of the GSVSC system; $\boldsymbol{u}_{\mathrm{GV}}=[U_{\mathrm{dc}}^{\mathrm{ref}}]$ is the control variable of the GSVSC system; $\boldsymbol{A}_{\mathrm{GV}}$ is the state matrix; and $\boldsymbol{B}_{\mathrm{GV}}$ is the control matrix.

C. DC System of MTDC

In steady-state analysis, the DC power flow is determined by the line resistances and the voltage drop differences between the interconnected DC buses. The current injection of the i^{th} DC bus $I_{\mathrm{dc},i}$ can be expressed as [19]:

$$I_{\mathrm{dc},i}=\sum_{j=1}^{n}G_{\mathrm{dc},ij}\,(u_{\mathrm{dc},i}-u_{\mathrm{dc},j}) \tag{10}$$

where $G_{\mathrm{dc},ij}$ is the conductivity between node i and node j of the MTDC system; $u_{\mathrm{dc},i}$ is the DC-side voltage of the i^{th} WFVSC; and $u_{\mathrm{dc},j}$ is the DC-side voltage of the j^{th} GSVSC. The active power of the i^{th} WFVSC that injects to the MTDC system can be written as:

$$P_{\mathrm{dc},i}=u_{\mathrm{dc},i}I_{\mathrm{dc},i} \tag{11}$$

Similarly, the active power that transfers to the AC grid through the i^{th} GSVSC can be obtained as:

$$P_{\mathrm{dc},i}=-u_{\mathrm{dc},i}I_{\mathrm{dc},i} \tag{12}$$

$P_{\mathrm{dc},i}$ of the MTDC system can be rewritten by combining (10)-(12) as:

$$P_{\mathrm{dc},i}=\begin{cases} u_{\mathrm{dc},i}\sum_{j=1}^{n}G_{\mathrm{dc},ij}(u_{\mathrm{dc},i}-u_{\mathrm{dc},j}) & i\in\mathcal{M} \\ -u_{\mathrm{dc},i}\sum_{j=1}^{n}G_{\mathrm{dc},ij}(u_{\mathrm{dc},i}-u_{\mathrm{dc},j}) & i\in\mathcal{W} \end{cases} \tag{13}$$

where $|\mathcal{M}|+|\mathcal{W}|=n$ is the total number of VSCs in the MTDC system.

$P_{\mathrm{dc},i}$ from the i^{th} WFVSC to MTDC is obtained according to Taylor expansion of (13), which is described as:

$$\begin{aligned} P_{\mathrm{dc},i}=&\,u_{\mathrm{dc},i}(t_0)\sum_{j=1}^{\mathcal{W}}G_{\mathrm{dc},ij}u_{\mathrm{dc},j}+u_{\mathrm{dc},i}\sum_{j=1}^{\mathcal{W}}G_{\mathrm{dc},ij}u_{\mathrm{dc},j}(t_0)- \\ &u_{\mathrm{dc},i}(t_0)\sum_{j=1}^{\mathcal{W}}G_{\mathrm{dc},ij}u_{\mathrm{dc},j}(t_0)\quad i\in\mathcal{M} \end{aligned} \tag{14}$$

D. Model of WF

The active and reactive power outputs of WT can be adjusted independently by the equipped full power converter with the decoupling control of the converter. $\boldsymbol{P}_{\mathrm{W}}$ and $\boldsymbol{Q}_{\mathrm{W}}$ are the active and reactive power current measurements, respectively. By defining the active and reactive power increment vectors as $\Delta \boldsymbol{P}_{\mathrm{W}}^{\mathrm{ref}}=\boldsymbol{P}_{\mathrm{W}}^{\mathrm{ref}}-\boldsymbol{P}_{\mathrm{W}}(t_0)$ and $\Delta \boldsymbol{Q}_{\mathrm{W}}^{\mathrm{ref}}=\boldsymbol{Q}_{\mathrm{W}}^{\mathrm{ref}}-\boldsymbol{Q}_{\mathrm{W}}(t_0)$, respectively, the dynamic of WTs can be represented as [10]:

$$\Delta \dot{\boldsymbol{P}}_{\mathrm{W}}=\frac{1}{1+s\boldsymbol{T}_{\mathrm{W}}^{P}}\Delta \boldsymbol{P}_{\mathrm{W}}^{\mathrm{ref}} \tag{15}$$

$$\Delta \dot{\boldsymbol{Q}}_{\mathrm{W}}=\frac{1}{1+s\boldsymbol{T}_{\mathrm{W}}^{Q}}\Delta \boldsymbol{Q}_{\mathrm{W}}^{\mathrm{ref}} \tag{16}$$

where $\boldsymbol{T}_{\mathrm{W}}^{P}$ and $\boldsymbol{T}_{\mathrm{W}}^{Q}$ are the time vectors of active and reactive control loops, respectively.

The continuous state space model of WF can be described as:

$$\dot{\boldsymbol{x}}_{\mathrm{WF}}=\boldsymbol{A}_{\mathrm{WF}}\boldsymbol{x}_{\mathrm{WF}}+\boldsymbol{B}_{\mathrm{WF}}\boldsymbol{u}_{\mathrm{WF}} \tag{17a}$$

$$\boldsymbol{x}_{\mathrm{WF}}=[\Delta P_{\mathrm{W1}},\Delta P_{\mathrm{W2}},...,\Delta P_{\mathrm{W}N_{\mathrm{w}}},\Delta Q_{\mathrm{W1}},\Delta Q_{\mathrm{W2}},...,\Delta Q_{\mathrm{W}N_{\mathrm{w}}}]^{\mathrm{T}} \tag{17b}$$

$$\boldsymbol{u}_{\mathrm{WF}}=[\Delta P_{\mathrm{W1}}^{\mathrm{ref}},\Delta P_{\mathrm{W2}}^{\mathrm{ref}},...,\Delta P_{\mathrm{W}N_{\mathrm{w}}}^{\mathrm{ref}},\Delta Q_{\mathrm{W1}}^{\mathrm{ref}},\Delta Q_{\mathrm{W2}}^{\mathrm{ref}},...,\Delta Q_{\mathrm{W}N_{\mathrm{w}}}^{\mathrm{ref}}]^{\mathrm{T}} \tag{17c}$$

$$\boldsymbol{A}_{\mathrm{WF}}=\mathrm{diag}\left(-\frac{1}{T_{\mathrm{W1}}^{P}},-\frac{1}{T_{\mathrm{W2}}^{P}},...,-\frac{1}{T_{\mathrm{W}N_{\mathrm{w}}}^{P}},-\frac{1}{T_{\mathrm{W1}}^{Q}},\right.$$
$$\left.-\frac{1}{T_{\mathrm{W2}}^{Q}},...,-\frac{1}{T_{\mathrm{W}N_{\mathrm{w}}}^{Q}}\right) \tag{17d}$$

$$\boldsymbol{B}_{\mathrm{WF}}=\mathrm{diag}\left(\frac{1}{T_{\mathrm{W1}}^{P}},\frac{1}{T_{\mathrm{W2}}^{P}},...,\frac{1}{T_{\mathrm{W}N_{\mathrm{w}}}^{P}},\frac{1}{T_{\mathrm{W1}}^{Q}},\frac{1}{T_{\mathrm{W2}}^{Q}},...,\frac{1}{T_{\mathrm{W}N_{\mathrm{w}}}^{Q}}\right) \tag{17e}$$

where $\boldsymbol{x}_{\mathrm{WF}}$ and $\boldsymbol{u}_{\mathrm{WF}}$ are the state and control variable vectors of the WF system, respectively; and $\boldsymbol{A}_{\mathrm{WF}}$ and $\boldsymbol{B}_{\mathrm{WF}}$ are the state and control matrixes, respectively.

The WF controlled AC bus voltage increment Δu_{S} can be affected by the terminal voltage increment Δu_{C} of WFVSC and the WT power outputs, which is expressed as:

$$\Delta u_{\mathrm{S}}\approx\frac{\partial u_{\mathrm{S}}}{\partial \boldsymbol{P}_{\mathrm{W}}^{\mathrm{T}}}\Delta \boldsymbol{P}_{\mathrm{W}}+\frac{\partial u_{\mathrm{S}}}{\partial \boldsymbol{Q}_{\mathrm{W}}^{\mathrm{T}}}\Delta \boldsymbol{Q}_{\mathrm{W}}+\frac{\partial u_{\mathrm{S}}}{\partial u_{\mathrm{C}}}\Delta u_{\mathrm{C}} \tag{18}$$

where $\partial u_{\mathrm{S}}/\partial \boldsymbol{P}_{\mathrm{W}}^{\mathrm{T}}$, $\partial u_{\mathrm{S}}/\partial \boldsymbol{Q}_{\mathrm{W}}^{\mathrm{T}}$, and $\partial u_{\mathrm{S}}/\partial u_{\mathrm{C}}$ are the sensitivity coefficients of the WF-controlled AC bus voltage with respect to active power vector $\boldsymbol{P}_{\mathrm{W}}$, reactive power vector $\boldsymbol{Q}_{\mathrm{W}}$, and WFVSC terminal voltage, respectively.

E. Model of Entire System

The continuous state space model of the entire system can be formulated as (19), and the detailed expressions can be found in Supplementary Material A.

$$\begin{cases}\dot{\boldsymbol{x}}=\boldsymbol{Ax}+\boldsymbol{Bu}+\boldsymbol{E}\\ \boldsymbol{y}=\boldsymbol{Cx}\end{cases} \tag{19}$$

IV. DOVC FOR MTDC SYSTEM WITH LARGE-SCALE WF CLUSTER BASED ON ADMM

A. Cost Function

For the MTDC system with large-scale WF cluster, the interaction between the MTDC system and WF cluster poses significant challenges for system controllers. Several factors must be considered to enhance the overall performance of the system, including minimizing grid power losses in the MTDC system and WF cluster, maintaining the voltages of WTs within each WF close to their rated levels, and achieving optimal active power distribution among the WFs. The WF control system is designed with three key control objectives.

1) The first control objective is the power loss of the WF, which can be calculated by:

$$\min f_1=\sum_{k=1}^{N_{\mathrm{P}}}\left\|\hat{P}_{\mathrm{loss}}^{\mathrm{WF}}(k)\right\|_2^2 \tag{20}$$

$$\hat{P}_{\mathrm{loss}}^{\mathrm{WF}}(k)=\frac{\partial P_{\mathrm{loss}}^{\mathrm{WF}}}{\partial \boldsymbol{P}_{\mathrm{W}}^{\mathrm{T}}}\Delta \boldsymbol{P}_{\mathrm{W}}(k)+\frac{\partial P_{\mathrm{loss}}^{\mathrm{WF}}}{\partial \boldsymbol{Q}_{\mathrm{W}}^{\mathrm{T}}}\Delta \boldsymbol{Q}_{\mathrm{W}}(k)+\frac{\partial P_{\mathrm{loss}}^{\mathrm{WF}}}{\partial u_{\mathrm{C}}}\Delta u_{\mathrm{C}}(k)+$$
$$P_{\mathrm{loss}}^{\mathrm{WF}}(t_0) \tag{21}$$

$$P_{\mathrm{loss}}^{\mathrm{WF}}(t_0)=\sum_{i=1}^{N}\sum_{j=1}^{N}V_iV_jG_{ij}\cos\theta_{ij} \tag{22}$$

where $P_{\mathrm{loss}}^{\mathrm{WF}}(k)$ is the power loss at time k; $\hat{P}_{\mathrm{loss}}^{\mathrm{WF}}(k)$ is the prediction value of power loss at time k; $\partial P_{\mathrm{loss}}^{\mathrm{WF}}/\partial \boldsymbol{P}_{\mathrm{W}}^{\mathrm{T}}$, $\partial P_{\mathrm{loss}}^{\mathrm{WF}}/\partial \boldsymbol{Q}_{\mathrm{W}}^{\mathrm{T}}$, and $\partial P_{\mathrm{loss}}^{\mathrm{WF}}/\partial u_{\mathrm{C}}$ are the sensitivity coefficients of the power loss of WF cluster to the active power vector of WTs, reactive power vector of WTs, and WFVSC terminal voltage, respectively; N_{P} is the prediction step; G_{ij} is the conductance between nodes i and j of the WF system with N nodes; and θ_{ij} is the phase angle difference between nodes i and j.

2) The second control objective is the WF bus voltage deviation $\Delta \hat{\boldsymbol{V}}_{\mathrm{W}}$ from the rated voltage.

$$\begin{cases}\min f_2=\sum_{k=1}^{N_{\mathrm{P}}}\left\|\Delta \hat{\boldsymbol{V}}_{\mathrm{W}}(k)\right\|_2^2\\ \Delta \hat{\boldsymbol{V}}_{\mathrm{W}}=[\Delta \hat{V}_{\mathrm{W1}},\Delta \hat{V}_{\mathrm{W2}},...,\Delta \hat{V}_{\mathrm{W}N_{\mathrm{w}}}]^{\mathrm{T}}\end{cases} \tag{23}$$

where $\Delta \hat{V}_{\mathrm{W}i}$ is the predictive value of voltage deviation of the i^{th} bus to its reference value $V_{\mathrm{W}i}^{\mathrm{ref}}$, which can be expressed by (24).

$$\Delta \hat{V}_{\mathrm{W}i}(k)=V_{\mathrm{W}i}(t_0)+\frac{\partial V_{\mathrm{W}i}}{\partial \boldsymbol{P}_{\mathrm{W}}^{\mathrm{T}}}\Delta \boldsymbol{P}_{\mathrm{W}}(k)+\frac{\partial V_{\mathrm{W}i}}{\partial \boldsymbol{Q}_{\mathrm{W}}^{\mathrm{T}}}\Delta \boldsymbol{Q}_{\mathrm{W}}(k)+$$
$$\frac{\partial V_{\mathrm{W}i}}{\partial u_{\mathrm{C}}}\Delta u_{\mathrm{C}}(k)-V_{\mathrm{W}i}^{\mathrm{ref}} \tag{24}$$

where $V_{\mathrm{W}i}(t_0)$ is the voltage measurement of the i^{th} bus at the initial time t_0; $\partial V_{\mathrm{W}i}/\partial \boldsymbol{P}_{\mathrm{W}}^{\mathrm{T}}$, $\partial V_{\mathrm{W}i}/\partial \boldsymbol{Q}_{\mathrm{W}}^{\mathrm{T}}$, and $\partial V_{\mathrm{W}i}/\partial u_{\mathrm{C}}$ are the sensitivity coefficients of the voltage of the i^{th} bus related to the active power vector, reactive power vector, and slack bus voltage, respectively.

3) When WT tracks active power based on the proportional distribution (PD) strategy, the maximum available active power of each WT is taken into account, and its available reactive capacity can be maximized. The active power of each WT should be as close as possible to the scheduling result of the PD strategy. The third cost function can be written as:

$$\begin{cases}\min f_3=\sum_{k=1}^{N_{\mathrm{P}}}\left\|\Delta \boldsymbol{P}_{\mathrm{W}}^{\mathrm{PD}}(k)\right\|_2^2\\ \Delta \boldsymbol{P}_{\mathrm{W}}^{\mathrm{PD}}=[\Delta P_{\mathrm{W1}}^{\mathrm{PD}},\Delta P_{\mathrm{W2}}^{\mathrm{PD}},...,\Delta P_{\mathrm{W}N_{\mathrm{w}}}^{\mathrm{PD}}]^{\mathrm{T}}\end{cases} \tag{25}$$

The deviation between the active power output of the i^{th}

WT and PD distributed active power of the i^{th} WT ΔP_{Wi}^{PD} can be calculated by:

$$\Delta P_{Wi}^{PD}(k)=P_{Wi}(t_0)+\Delta P_{Wi}(k)-\alpha_i P_{WF}^{ref} \tag{26}$$

where P_{Wi} is the active power output of the i^{th} WT; ΔP_{Wi} is the active power output increment of the i^{th} WT; P_{WF}^{ref} is the reference value of the WF active power output; and α_i is the active power scale factor of the i^{th} WT calculated by (27).

$$\alpha_i=\frac{P_{Wi}^{avi}}{\sum_{i=1}^{N_W} P_{Wi}^{avi}} \tag{27}$$

where P_{Wi}^{avi} is the available active power of the i^{th} WT.

To reduce the power loss of the entire system and improve its economy, the control objective of MTDC focuses on the active power loss of the MTDC system:

$$\min f_4=\sum_{k=1}^{N_P} P_{loss}^{dc}(k) \tag{28}$$

$$P_{loss}^{dc}(k)=\boldsymbol{u}_{dc}^{T}(k)\boldsymbol{G}_{dc}\boldsymbol{u}_{dc}(k) \tag{29}$$

where $\boldsymbol{u}_{dc}=[u_{dc,1},u_{dc,2},u_{dc,3},...,u_{dc,n}]^T$ is the DC-side voltage vector of VSCs in the MTDC system; and $\boldsymbol{G}_{dc}$ is the DC-side control matrix.

According to (20), (23), (26), and (28), the overall cost function of the MTDC system is obtained as:

$$\min f=\left(\lambda_1\sum_{m=1}^{|\mathcal{M}|} f_1^m+\lambda_2\sum_{m=1}^{|\mathcal{M}|} f_2^m+\lambda_3\sum_{m=1}^{|\mathcal{M}|} f_3^m+\lambda_4 f_4\right) \tag{30}$$

where λ_1, λ_2, λ_3, and λ_4 are the weighting coefficients for f_1, f_2, f_3, and f_4, respectively.

B. Constraints

1) WF system constraints: the active power and reactive power of WTs in WF are constrained by:

$$-P_{Wi}(t_0)\le\Delta P_{Wi}(k)\le P_{Wi}^{avi}-P_{Wi}(t_0)\quad i\in N_W \tag{31}$$

$$Q_{Wi}^{min}-Q_{Wi}(t_0)\le\Delta Q_{Wi}(k)\le Q_{Wi}^{max}-Q_{Wi}(t_0) \tag{32}$$

where Q_{Wi} is the reactive power output of the i^{th} WT; $\Delta Q_{Wi}(k)$ is the reactive power output increment of the i^{th} WT at time k; and Q_{Wi}^{min} and Q_{Wi}^{max} are the minimum and maximum available reactive power of the i^{th} WT, respectively.

The output power flow of the i^{th} WF to the DC system $P_{WF,i}(k)$ can be expressed by:

$$P_{WF,i}(k)=\sum_{j=1}^{N_W}(P_{Wj}(t_0)+\Delta P_{Wj}(k))-P_{loss}^{WF,i}(k) \tag{33}$$

where $P_{loss}^{WF,i}(k)$ is the power loss of the i^{th} WF at time k.

The terminal voltage increment of the i^{th} WFVSC $\Delta u_{C,i}$ is constrained by:

$$u_{C,i}^{min}-u_{C,i}(t_0)\le\Delta u_{C,i}(k)\le u_{C,i}^{max}-u_{C,i}(t_0) \tag{34}$$

where $u_{C,i}$ is the terminal voltage of the i^{th} WFVSC; and $u_{C,i}^{min}$ and $u_{C,i}^{max}$ are the minimum and maximum terminal voltages of the i^{th} WFVSC, respectively.

2) MTDC system constraints: the active power flow between the k^{th} WFVSC and j^{th} GSVSC is constrained by:

$$0<-u_{dc,k}G_{dc,kj}u_{dc,j}<P_{dc,kj}^{rate} \tag{35}$$

where $P_{dc,kj}^{rate}$ is the rated active power of the DC cable connecting the k^{th} WFVSC and the j^{th} GSVSC.

The GSVSC is required to track the WF power reference from system operators. The PI-based dynamic controller is introduced to eliminate the active power output error of i^{th} GSVSC $\Delta P_{GS,i}$ caused by the inaccuracy of the system model and disturbances. The active power equality constraint of the i^{th} GSVSC can be described by:

$$P_{GS,i}^{ref}(k)=P_{TSO,i}^{ref}+\Delta P_{GS,i}(k) \tag{36}$$

$$P_{GS,i}^{ref}(k)=-u_{dc,i}(t_0)\sum_{j=1}^{n}G_{dc,ij}u_{dc,j}^{ref}(k)-u_{dc,i}^{ref}(k)\sum_{j=1}^{n}G_{dc,ij}u_{dc,j}(t_0)+ u_{dc,i}(t_0)\sum_{j=1}^{n}G_{dc,ij}u_{dc,j}(t_0)\quad i\in\mathcal{W} \tag{37}$$

$$\Delta P_{GS,i}(k)=\Delta P_{GS,i}^{0}+\beta(P_{TSO,i}^{ref}-P_{GS,i}^{meas}(t_0)) \tag{38}$$

$$\Delta P_{GS,i}^{0}=P_{TSO,i}^{ref,0}-P_{GS,i}^{meas,0} \tag{39}$$

where $P_{GS,i}^{ref}$ and $P_{GS,i}^{meas}$ are the active power reference and measurement transferred to the AC grid through the i^{th} GSVSC, respectively; $\Delta P_{GS,i}^{0}$ is the difference between the scheduling command for active power output of the GSVSC and the active power output measurement of GSVSC at the previous control instant; $P_{TSO,i}^{ref,0}$ and $P_{GS,i}^{meas,0}$ are the scheduling command and measurement of the active power output for the i^{th} GSVSC at the previous control instant, respectively; and β is the PI controller coefficient.

$u_{dc,i}$ is constrained by:

$$u_{dc,i}^{min}\le u_{dc,i}\le u_{dc,i}^{max}\quad i\in n \tag{40}$$

where $u_{dc,i}^{min}$ and $u_{dc,i}^{max}$ are the minimum and maximum DC-side voltages of the i^{th} VSC, respectively.

C. ADMM-based Solution Method for Entire System

With the continuous expansion of MTDC system and WF cluster, the optimization problem for the entire system evolves into a large-scale, multi-input, multi-output optimization problem with extensive constraints. Utilizing a centralized solution method places a significant computational burden on the central controller, making real-time control difficult to achieve.

To reduce computational burden, an ADMM-based solution method is proposed for the DOVC strategy. The DOVC strategy distributes the computational tasks between the MTDC controller and the individual WF controllers. The optimization problem is decomposed into separate parts for the MTDC and each WF, with the WFVSC active power outputs serving as the common variables. Consequently, the optimization problem (30) can be distributed to the MTDC controller and WF controllers and processed in parallel while ensuring global optimality [27], [28]. The total cost function is obtained by:

$$\begin{cases}\min f=\left(\lambda_1\sum_{m=1}^{|\mathcal{M}|} f_1^m+\lambda_2\sum_{m=1}^{|\mathcal{M}|} f_2^m+\lambda_3\sum_{m=1}^{|\mathcal{M}|} f_3^m+\lambda_4 f_4\right)\\ \text{s.t. } P_{dc,m}(k)=P_{WF,m}(k)\quad m\in\mathcal{M}\\ \qquad \sum_{m=1}^{\mathcal{M}}P_{dc,m}(k)=\sum_{j=1}^{\mathcal{W}}P_{GS,j}(k)+P_{loss}^{dc}(k)\\ \qquad (31)-(40)\end{cases} \tag{41}$$

where $P_{\mathrm{dc},m}(k)$ and $P_{\mathrm{WF},m}(k)$ are the boundary active power flows of the k^{th} WFVSC obtained by the MTDC controller and the k^{th} WF controller, respectively; $P_{\mathrm{GS},j}(k)$ is the active power output of the j^{th} GSVSC; and $P_{\mathrm{loss}}^{\mathrm{dc}}(k)$ is the power loss of DC system at time k.

By defining the global variable $\boldsymbol{Z}=[P_{\mathrm{WF},1}, P_{\mathrm{WF},2}, \dots, P_{\mathrm{WF},\mathcal{M}}]^{\mathrm{T}}$ as the active power output vector of the WFs, $\boldsymbol{Z}_l$ as the local variable vector obtained by the WF controllers, and $\boldsymbol{Z}_g$ as the global variable vector obtained by the MTDC controller, the augmented Lagrangian function can be described as:

$$\min\left\{\lambda_1\sum_{m=1}^{|\mathcal{M}|}f_1^m+\lambda_2\sum_{m=1}^{|\mathcal{M}|}f_2^m+\lambda_3\sum_{m=1}^{|\mathcal{M}|}f_3^m+\lambda_4 f_4+\boldsymbol{\gamma}^{\mathrm{T}}(\boldsymbol{Z}_l-\boldsymbol{Z}_g)+\frac{\boldsymbol{\rho}}{2}\left\|\boldsymbol{Z}_l-\boldsymbol{Z}_g\right\|^2\right\} \tag{42}$$

where $\boldsymbol{\rho}$ is the penalty factor vector; and $\boldsymbol{\gamma}$ is the dual-variable vector.

The k^{th} variable of $\boldsymbol{Z}_l$, $Z_{l,k}$, can be obtained from the augmented Lagrangian for the k^{th} WF controller.

$$\min\left\{\lambda_1 f_1^k+\lambda_2 f_2^k+\lambda_3 f_3^k+\gamma_k(Z_{l,k}-Z_{g,k})+\frac{\rho_k}{2}\left\|Z_{l,k}-Z_{g,k}\right\|^2\right\} \tag{43}$$

where $Z_{g,k}$ is the k^{th} variable of global variable vector $\boldsymbol{Z}_g$; and γ_k and ρ_k are the dual-variable and penalty factor of the k^{th} WF controller, respectively.

The initial values of $\boldsymbol{Z}_g$ and $\boldsymbol{Z}_l$ are set to be 0. The $(r+1)^{\mathrm{th}}$ iteration process is as follows.

1) The MTDC controller only needs to solve the power loss optimization problem of the DC system. The DC-side voltage reference vector of VSCs $\boldsymbol{u}_{\mathrm{dc}}^{\mathrm{ref}}$ and global variable vector $\boldsymbol{Z}_g$ can be updated by:

$$\begin{cases}(\boldsymbol{u}_{\mathrm{dc}}^{\mathrm{ref}},\boldsymbol{Z}_g)^{r+1}:=\arg\min\left\{\lambda_4 f_4(\boldsymbol{u}_{\mathrm{dc}})+(\boldsymbol{\gamma}^r)^{\mathrm{T}}(\boldsymbol{Z}_l^r-\boldsymbol{Z}_g)+\dfrac{\rho}{2}\left\|\boldsymbol{Z}_l^r-\boldsymbol{Z}_g\right\|^2\right\}\\ \text{s.t. } (35)\text{-}(40)\end{cases} \tag{44}$$

where the superscript r denotes the iteration step.

2) The k^{th} variable of $\boldsymbol{Z}_g$, $Z_{g,k}^{r+1}$, is obtained from the MTDC controller. $\Delta\boldsymbol{u}_{\mathrm{WF},k}$ and $Z_{l,k}$ can be updated in the k^{th} WF controller by:

$$\begin{cases}(\Delta\boldsymbol{u}_{\mathrm{WF},k},Z_{l,k})^{r+1}:=\arg\min\left\{\lambda_1 f_1(\Delta\boldsymbol{u}_{\mathrm{WF},k})+\lambda_2 f_2(\Delta\boldsymbol{u}_{\mathrm{WF},k})+\lambda_3 f_3(\Delta\boldsymbol{u}_{\mathrm{WF},k})+\gamma_k^r(Z_{l,k}-Z_{g,k}^{r+1})+\dfrac{\rho_k}{2}\left\|Z_{l,k}-Z_{g,k}^{r+1}\right\|^2\right\}\\ \Delta\boldsymbol{u}_{\mathrm{WF},k}=[\Delta u_{\mathrm{C}}^{\mathrm{ref},k},\Delta P_{\mathrm{W1}}^{\mathrm{ref},k},\dots,\Delta P_{\mathrm{WN_w}}^{\mathrm{ref},k},\Delta Q_{\mathrm{W1}}^{\mathrm{ref},k},\dots,\Delta Q_{\mathrm{WN_w}}^{\mathrm{ref},k}]^{\mathrm{T}}\\ \text{s.t. } (31)\text{-}(34)\end{cases} \tag{45}$$

3) γ_k^{r+1} is also updated in the k^{th} WF controller, which can be updated by:

$$\gamma_k^{r+1}:=\gamma_k^r+\rho_k^r(Z_{l,k}^{r+1}-Z_{g,k}^{r+1}) \tag{46}$$

Then, the dynamic ρ_k is updated. With $\boldsymbol{J}$ as the primal residual vector and $\boldsymbol{h}$ as the dual residual vector, J_k and h_k are the k^{th} variables of $\boldsymbol{J}$ and $\boldsymbol{h}$, respectively.

$$h_k^{r+1}=Z_{l,k}^{r+1}-Z_{g,k}^{r+1} \tag{47}$$

$$J_k^{r+1}=\rho_k^r(Z_{g,k}^{r+1}-Z_{g,k}^r) \tag{48}$$

$$\rho_k^{r+1}:=\begin{cases}\xi\rho_k^r & \left\|h_k^{r+1}\right\|^2\geq\varepsilon\left\|J_k^{r+1}\right\|^2\\ \dfrac{\rho_k^r}{\varpi} & \left\|h_k^{r+1}\right\|^2\leq\varepsilon\left\|J_k^{r+1}\right\|^2\\ \rho_k^r & \text{otherwise}\end{cases} \tag{49}$$

where ξ, ε, and ϖ are the penalty coefficients.

4) The convergence is checked by:

$$\begin{cases}0\leq\left\|J_k^{r+1}\right\|^2\leq\delta^{\mathrm{pri}}\\ 0\leq\left\|h_k^{r+1}\right\|^2\leq\delta^{\mathrm{dual}}\end{cases} \tag{50}$$

where δ^{pri} and δ^{dual} are the tolerable boundaries of J_k and h_k, respectively.

The flowchart of the proposed ADMM-based solution method is shown in Fig. 8.

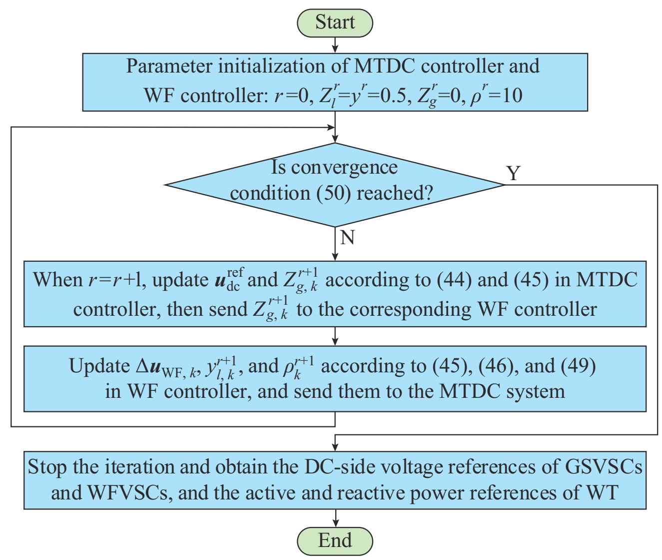

Fig. 8. Flowchart of proposed ADMM-based solution method.

V. Simulation Results

A. Test Platform and System Parameters

The structure of the testbed system is shown in Fig. 9. The MTDC system with large-scale WF cluster includes 3 WFVSCs and 2 GSVSCs. The 1st, 2nd, and 3rd WFs consist of 24×5 MW WTs, 16×5 MW WTs, and 24×5 MW WTs, respectively. The case study is tested in MATLAB/Simulink. The parameters of the electric system are shown in Table I, where R, L, C, X, and S_n denote resistance, inductance, capacitance, reactance, and rated capacity, respectively.

B. Control Performance of Proposed DOVC Strategy

To evaluate the performance of the proposed DOVC strategy, two traditional control strategies are selected for comparison: the centralized optimal voltage control (COVC) strategy and the two-tier optimal control (TOC) strategy.

1) In the COVC strategy, all optimization problems are solved by a central controller.

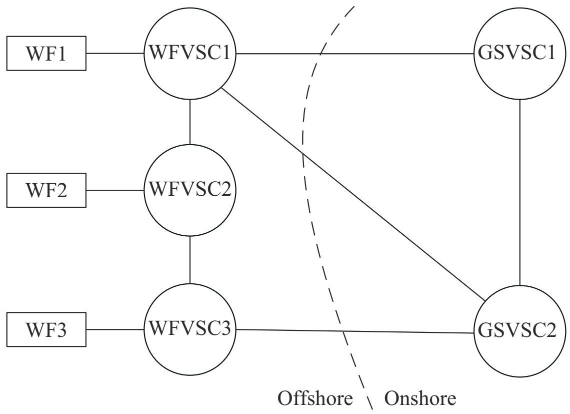

Fig. 9. Structure of testbed system.

TABLE I
PARAMETER OF ELECTRIC SYSTEM

Equipment	Parameter
33 kV cable	$R=0.078$ Ω/km, $L=0.39$ mH/km, $C=0.25$ μF/km
155 kV cable	$R=0.0108$ Ω/km, $L=0.47$ mH/km, $C=0.13$ μF/km
400 kV cable	$R=0.0144$ Ω/km
33 kV/155 kV transformer	$S_n=200$ MVA, $R=0.001$ p.u., $X=0.06$ p.u.
0.9 kV/33 kV transformer	$S_n=6.25$ MVA, $R=0.008$ p.u., $X=0.06$ p.u.
HVDC converter	$S_n=200$ MVA
WT converter	$S_n=6.25$ MVA

2) In the TOC strategy, the optimization problem of the MTDC system with large-scale WF cluster is divided into two independent optimization problems that are solved sequentially. One focuses on optimizing the MTDC system, while the other addresses the WF optimization problems.

Figure 10 shows the active power output tracking performance of GSVSC with the proposed DOVC strategy. During 0-160 s, the dispatch commands of GSVSC1 and GSVSC2 are set to be 120 MW and 100 MW, respectively. During 160-245 s, the dispatch commands are changed to be 140 MW and 70 MW, respectively. After 245 s, the active power remains constant at 140 MW and 70 MW. All WTs operate at the maximum available power during 290-550 s. In Fig. 10(a), the proposed DOVC strategy with error elimination control demonstrates excellent active power tracking performance, especially during 290-550 s, where there is almost no fluctuation in active power. Figure 10(b) shows the active power output tracking performance without error elimination, where the tracking error is around 0.05 MW, indicating that active power output tracking has not been fully achieved. This suggests that error elimination control plays a critical role in enabling the proposed DOVC strategy to achieve fast and accurate active power reference tracking.

The active power losses with DOVC, COVC, and TOC strategies are shown in Fig. 11. Since the TOC strategy employs a two-tier control structure, it struggles to achieve global optimal operation for the entire system.

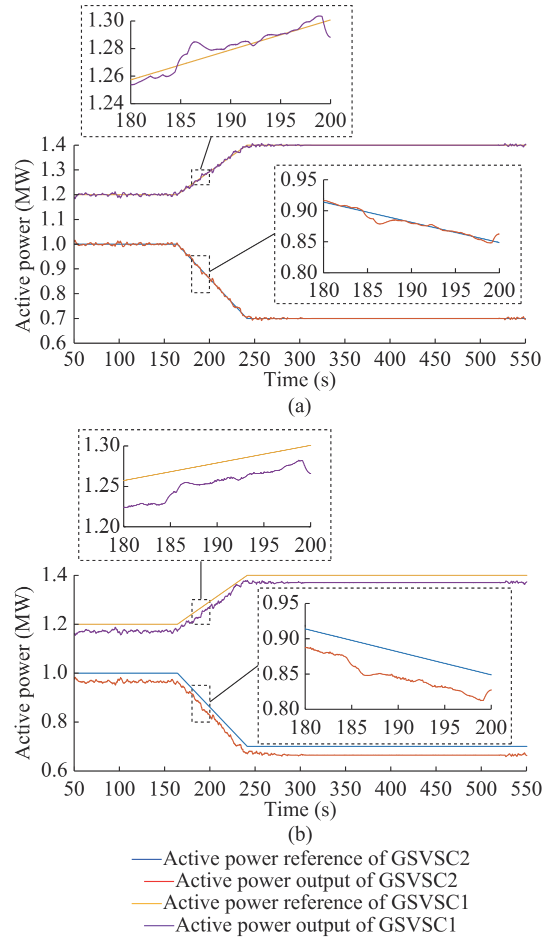

Fig. 10. Active power output tracking performance of GSVSC with proposed DOVC strategy. (a) With error elimination. (b) Without error elimination.

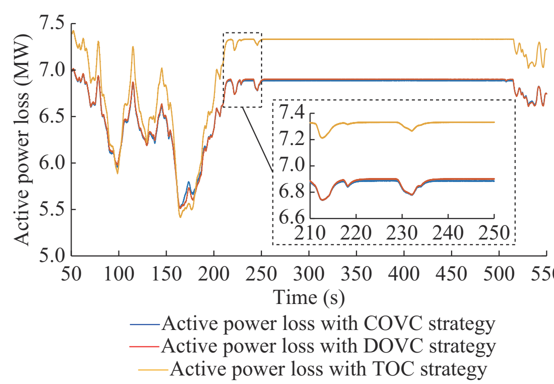

Fig. 11. Active power losses with DOVC, COVC, and TOC strategies.

Figure 11 shows that the active power loss using the DOVC and COVC strategies is lower than that using the TOC strategy. Especially during 290-550 s, the active power loss with the DOVC and COVC strategies is 0.4 MW lower than that with TOC strategy. Simulation results show that the proposed DOVC strategy can achieve power loss optimization compared with the COVC strategy.

In Fig. 12(a), the voltages of WT12 in WF1 are presented, which is located at the end of the feeder. Figure 12(b) shows the voltage of WT8 in WF2. As shown in Fig. 12(a), the voltages applying the DOVC and COVC strategies are closer to the rated voltage of 33 kV with the maximum deviations of approximately 0.25 kV and 0.5 kV, respectively. These deviations are significantly lower than 0.87 kV observed with the TOC strategy. As shown in Fig. 12(b), the voltage deviations from the rated value using DOVC and COVC strategies are 0.15 kV and 0.003 kV, respectively, which are much lower than the voltage deviation of 0.7 kV with TOC strategy. These results indicate that the DOVC and COVC strategies provide superior voltage regulation performance compared with the TOC strategy, suggesting that the system operates with greater stability and robustness under varying wind speeds.

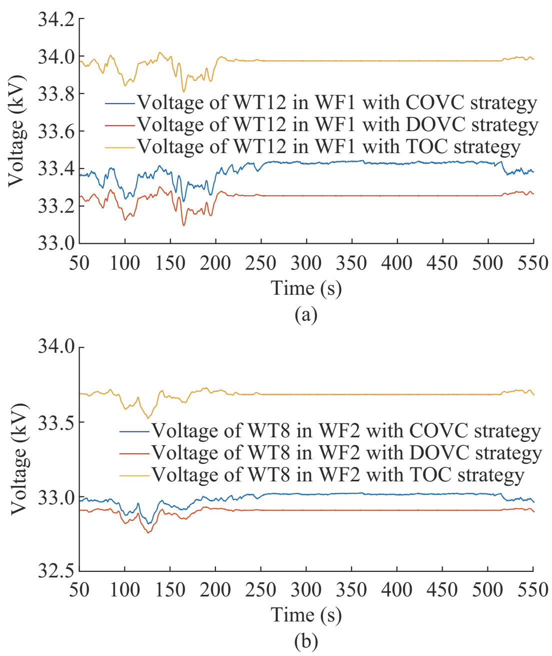

Fig. 12. Voltages of WTs with DOVC, COVC, and TOC strategies. (a) Voltage of WT12 in WF1. (b) Voltage of WT8 in WF2.

Figure 13 shows the DC-side voltage of the GSVSC2 with DOVC, COVC, and TOC strategies. Since COVC strategy is a centralized control strategy that guarantees global optimality, the voltage curves with the proposed DOVC strategy closely resemble those of the COVC strategy. This similarity implies that the proposed DOVC strategy can also achieve global optimal operation. In contrast, the TOC strategy, which has different control objectives and does not account for the power loss of DC lines connected to GSVSC2, results in a slightly lower voltage compared with the DOVC and COVC strategies.

Figure 14 shows the iteration curves of Z_l and Z_g during the DOVC iteration process. As illustrated, $Z_{l,k}$ and $Z_{g,k}$ converge to the same value, reaching the optimal solution within approximately 7 iterations, indicating rapid convergence. The ADMM-based solution method has fewer iterations and lower computational burden, ensuring real-time control of MTDC systems with large-scale WF cluster. Consequently, the proposed DOVC strategy fully satisfies the quick response requirement of the system.

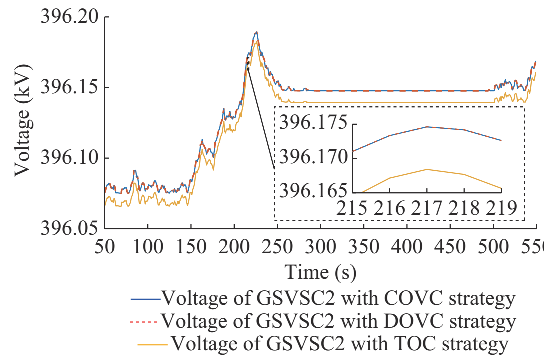

Fig. 13. DC-side voltage of GSVSC2 with DOVC, COVC, and TOC strategies.

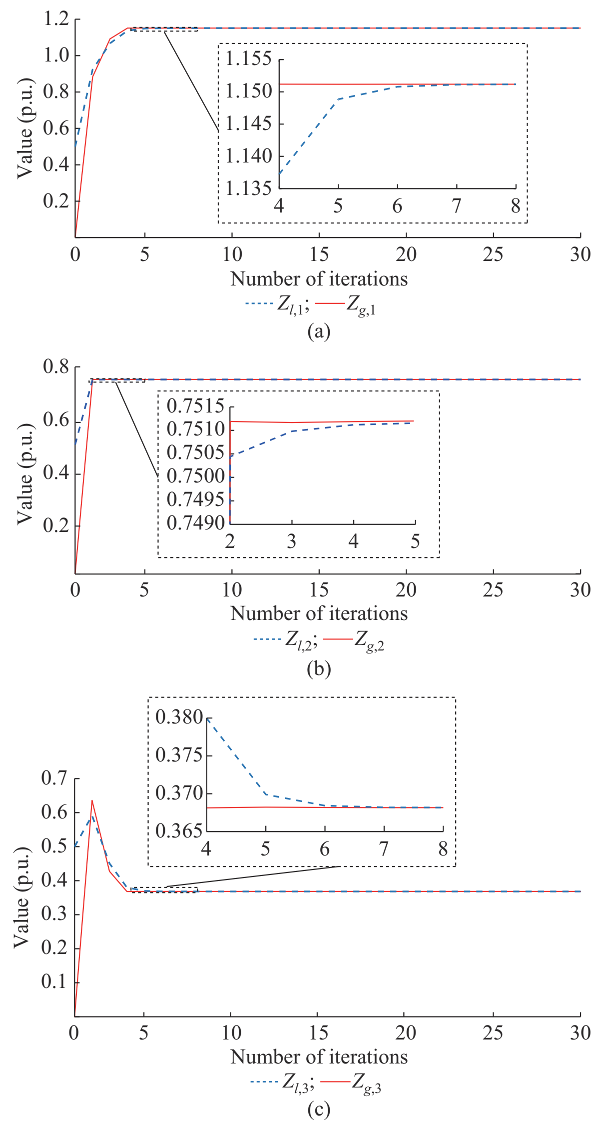

Fig. 14. Iteration curves of Z_l and Z_g. (a) $Z_{l,1}$ and $Z_{g,1}$. (b) $Z_{l,2}$ and $Z_{g,2}$. (c) $Z_{l,3}$ and $Z_{g,3}$.

We test the proposed DOVC, COVC, and TOC strategies using 64 WTs, 128 WTs, and 256 WTs on a personal computer (Intel Core i7-11700KF, 32 GB RAM). The comparison of computation time is presented in Table II. It can be observed that the COVC strategy suffers from heavy centralized computation with the increase of WTs. When the number of WTs increases to 256, the computation time is 32.709 s, representing an increase of 3286% compared with a system with 64 WTs.

TABLE II
COMPARISON OF COMPUTATION TIME FOR THREE STRATEGIES

Strategy	Computation time (s)		
	64 WTs	128 WTs	256 WTs
COVC	0.966	4.881	32.709
TOC	0.841	3.164	25.125
DOVC	0.751	1.694	7.285

By decomposing the global optimization problem into smaller subproblems that can be solved in parallel, the proposed DOVC strategy strikes a balance between computational efficiency and optimized performance. The proposed DOVC strategy has shorter computation time than both COVC and TOC strategies, reducing computation time by 77.73% and 71%, respectively, for the system with 256 WTs. The proposed ADMM-based solution method demonstrates excellent scalability, avoiding the need for centralized computation and intensive data exchange, ensuring that the computation time remains manageable even when the size of the WF increases.

VI. CONCLUSION

This paper proposes DOVC strategy for MTDC system with large-scale WF cluster based on ADMM. The proposed DOVC strategy optimizes system operation by minimizing power losses, reducing terminal voltage deviations of WTs, and achieving optimal active power distribution. The proposed ADMM-based solution method is used to decompose the large-scale optimization problem into several sub-optimization problems. The computational burden is reduced and the real-time control for the MTDC system with large-scale WF cluster can be ensured. Simulation results demonstrate that the proposed DOVC strategy achieves control performance compared with the COVC strategy in terms of minimizing voltage deviations and power losses while outperforming the TOC strategy. Additionally, as the scale of the WF increases, the computation time of the proposed DOVC strategy is significantly lower than that of the COVC strategy. The proposed DOVC strategy enhances the dynamic response, voltage stability, and overall efficiency of the MTDC system with large-scale WF cluster.

REFERENCES

[1] Z. Duan, Y. Meng, S. Yan *et al*., "Large-signal stability analysis for offshore wind power fractional frequency transmission system with modular multilevel matrix converter," *International Journal of Electrical Power and Energy Systems*, vol. 153, p. 109379, Nov. 2023.

[2] W. Liao, Q. Wu, H. Cui *et al*., "Model predictive control based coordinated voltage control for offshore radial DC-connected wind farms," *Journal of Modern Power Systems and Clean Energy*, vol. 11, no. 1, pp. 280-289, Jan. 2023.

[3] G. Lee, D. Kwon, S. Moon *et al*., "DC current and voltage droop control method of hybrid HVDC systems for an offshore wind farm connection to enhance AC voltage stability," *IEEE Transactions on Energy Conversion*, vol. 36, no. 1, pp. 468-479, Mar. 2021.

[4] X. Li, S. Huang, Y. Qu *et al*., "Decentralized optimal voltage control for wind farm with deep learning-based data-driven modeling," *International Journal of Electrical Power and Energy Systems*, vol. 161, p. 110195, Oct. 2024.

[5] B. Li, Q. Li, Y. Wang *et al*., "A novel method to determine droop coefficients of DC voltage control for VSC-MTDC system," *IEEE Transactions on Power Delivery*, vol. 35, no. 5, pp. 2196-2211, Oct. 2020.

[6] S. Khan and S. Bhowmick, "A generalized power-flow model of VSC based hybrid AC-DC systems integrated with offshore wind farms," *IEEE Transactions on Sustainable Energy*, vol. 10, no. 4, pp. 1775-1783, Oct. 2019.

[7] R. Yang, G. Shi, X. Cai *et al*., "Autonomous synchronizing and frequency response control of multi-terminal DC systems with wind farm integration," *IEEE Transactions on Sustainable Energy*, vol. 11, no. 4, pp. 2504-2514, Oct. 2020.

[8] L. Shi, G. P. Adam, R. Li *et al*., "Enhanced control of offshore wind farms connected to MTDC network using partially selective DC fault protection," *IEEE Journal of Emerging and Selected Topics in Power Electronics*, vol. 9, no. 3, pp. 2926-2935, Jun. 2021.

[9] Y. A. Sultan, S. S. Kaddah, and A. A. Eladl, "VSC-HVDC system-based on model predictive control integrated with offshore wind farms," *IET Renewable Power Generation*, vol. 15, no. 6, pp. 1315-1330, Feb. 2021.

[10] Y. Guo, H. Gao, Q. Wu *et al*., "Enhanced voltage control of VSC-HVDC connected offshore wind farms based on model predictive control," *IEEE Transactions on Sustainable Energy*, vol. 9, no. 1, pp. 474-487, Jan. 2018.

[11] S. Huang, Q. Wu, J. Zhao *et al*., "Distributed optimal voltage control for VSC-HVDC connected large-scale wind farm cluster based on analytical target cascading method," *IEEE Transactions on Sustainable Energy*, vol. 11, no. 4, pp. 2152-2161, Oct. 2020.

[12] B. Jeong, D. Kwon, J. Park *et al*., "Optimal secondary control to suppress voltage fluctuations in an HVDC-linked wind farm grid," *IEEE Transactions on Power Systems*, vol. 37, no. 4, pp. 2563-2577, Jul. 2022.

[13] S. Huang, P. Li, Q. Wu *et al*., "ADMM-based distributed optimal reactive power control for loss minimization of DFIG-based wind farms," *International Journal of Electrical Power and Energy Systems*, vol. 118, p. 105827, Jun. 2020.

[14] Y. Zhu, Y. Zhang, and Z. Wei, "Hierarchical cluster coordination control strategy for large-scale wind power based on model predictive control and improved multi-time-scale active power dispatching," *Journal of Modern Power Systems and Clean Energy*, vol. 11, no. 3, pp. 827-839, May 2023.

[15] S. Huang, Q. Wu, Y. Guo *et al*., "Distributed voltage control based ADMM for large-scale wind farm cluster connected to VSC-HVDC," *IEEE Transactions on Sustainable Energy*, vol. 11, no. 2, pp. 584-594, Apr. 2020.

[16] S. Huang, Q. Wu, W. Liao *et al*., "Adaptive droop-based hierarchical optimal voltage control scheme for VSC-HVDC connected offshore wind farm," *IEEE Transactions on Industrial Informatics*, vol. 17, no. 12, pp. 8165-8176, Dec. 2021.

[17] Z. Wang, J. He, Y. Xu *et al*., "Distributed control of VSC-MTDC systems considering tradeoff between voltage regulation and power sharing," *IEEE Transactions on Power Systems*, vol. 35, no. 3, pp. 1812-1821, May 2020.

[18] B. Zhang, F. Gao, D. Liao *et al*., "Distributed AC-DC coupled hierarchical control for VSC-based DC microgrids," *IEEE Transactions on Power Electronics*, vol. 39, no. 2, pp. 2180-2199, Feb. 2024.

[19] S. S. Sayed and A. M. Massoud, "A generalized approach for design of contingency versatile DC voltage droop control in multi-terminal HVDC networks," *International Journal of Electrical Power and Energy Systems*, vol. 126, p. 106413, Mar. 2021.

[20] Y. Wang, F. Qiu, G. Liu *et al*., "Adaptive reference power based voltage droop control for VSC-MTDC systems," *Journal of Modern Power Systems and Clean Energy*, vol. 11, no. 1, pp. 381-388, Jan. 2023.

[21] G. P. Adam, F. Alsokhiry, and A. Alabdulwahab, "DC grid controller for optimized operation of voltage source converter based multi-terminal HVDC networks," *Electric Power Systems Research*, vol. 202, p. 107595, Jan. 2022.

[22] X. Li, L. Guo, C. Hong *et al*., "Hierarchical control of multiterminal DC grids for large-scale renewable energy integration," *IEEE Transactions on Sustainable Energy*, vol. 9, no. 3, pp. 1448-1457, Jul. 2018.

[23] D. Kotur and P. Stefanov, "Optimal power flow control in the system with offshore wind power plants connected to the MTDC network," *International Journal of Electrical Power and Energy Systems*, vol.

105, pp. 142-150, Feb. 2019.

[24] Y. Zhang, X. Meng, A. M. Shotorbani *et al*., "Minimization of AC-DC grid transmission loss and DC voltage deviation using adaptive droop control and improved AC-DC power flow algorithm," *IEEE Transactions on Power Systems*, vol. 36, no. 1, pp. 744-756, Jan. 2021.

[25] P. Wang, Q. Wu, S. Huang *et al*., "ADMM-based distributed active and reactive power control for regional AC power grid with wind farms," *Journal of Modern Power Systems and Clean Energy*, vol. 10, no. 3, pp. 588-596, May 2022.

[26] R. Asif, Q. Huang, J. Li *et al*., "Hierarchical control scheme for VSC-MTDC system with multiple renewable energy sites based on optimal power flow and droop scheme," in *Proceedings of The 6th IEEE Conference on Energy Internet and Energy System Integration (EI2)*, Chengdu, China, May 2023, pp. 899-904.

[27] Y. Guo, H. Gao, H. Xing *et al*., "Decentralized coordinated voltage control for VSC-HVDC connected wind farms based on ADMM," *IEEE Transactions on Sustainable Energy*, vol. 10, no. 2, pp. 800-810, Apr. 2019.

[28] S. Huang, Q. Wu, W. Bao *et al*., "Hierarchical optimal control for synthetic inertial response of wind farm based on ADMM," *IEEE Transactions on Sustainable Energy*, vol. 12, no. 1, pp. 25-35, Jan. 2021.

Xueping Li received the B.S. degree from Xiangtan University, Xiangtan, China, in 2015, and the M.S. degree from Hunan University, Changsha, China, in 2018. She is currently working toward the Ph.D. degree in Hunan University. Her research interests include microgrid, wind power generation, and wind farm optimization.

Yinpeng Qu received the B.S. and Ph.D. degrees from Wuhan University, Wuhan, China, in 2013 and 2021, respectively. He is currently working as an Associate Professor in Hunan University, Changsha, China. His research interests include artificial intelligence, sustainable energy generation, and efficient operation of wind power plant.

Jianxin Deng received the B.S. and M.S. degrees from Hunan University, Changsha, China, in 2017 and 2020, respectively. He is currently working at Dongguan Power Supply Bureau, Guangdong Power Grid Co., Ltd., Guangzhou, China. His research interests include wind power generation, voltage control, and wind farm optimization.

Sheng Huang received the M.S. and Ph.D. degrees from Hunan University, Changsha, China, in 2012 and 2016, respectively. He was a Postdoc with the Center for Electric Power and Energy, Technical University of Denmark, Lyngby, Denmark, from 2017 to 2021. He is currently working as a Professor in Hunan University. His research interests include renewable energy generation, modeling and integration of wind power, control of energy storage systems, voltage control, generator, and motor control.

Derong Luo received the M.S. and Ph.D. degrees from Hunan University, Changsha, China, in 1990 and 2003, respectively. He is currently working as a Professor in Hunan University. His research interests include permanent magnet synchronous motor drives and position sensorless control of AC motors.

Qiuwei Wu received the Ph.D. degree in power system engineering from Nanyang Technological University, Singapore, in 2009. He is working in the School of Electronics, Electrical Engineering, and Computer Science, Queen's University Belfast, BT8 5BN, Belfast, UK. His research interests include operation and control of power systems with high penetration of renewables, wind power modelling and control, active distribution network, and operation of integrated energy system.